Published in final edited form as:
Biochemistry. 2013 September 3; 52(35): . doi:10.1021/bi400642u.

Structural Features of LC8-Induced Self Association of Swallow†

Ariam I. Kidane[1], **Yujuan Song**[1], **Afua Nyarko**[1], **Justin Hall**[1,3], **Michael Hare**[1], **Frank Löhr**[2], and **Elisar Barbar**[1,*]

[1]Department of Biochemistry and Biophysics, Oregon State University, Corvallis, OR 97331

[2]Institute of Biophysical Chemistry, Goethe-University, D-60438 Frankfurt, Germany

Abstract

Cell function depends on the collective activity of protein networks within which a few proteins, called hubs, participate in a large number of interactions. Dynein light chain LC8, first discovered as a subunit of the motor protein dynein, is considered to have a role broader than dynein and its participation in diverse systems fits the description of a hub. Among its partners is Swallow with which LC8 is essential for proper localization of *bicoid* mRNA at the anterior cortex of *Drosophila* oocytes. Why LC8 is essential in this process is not clear, but emerging evidence suggests that LC8 functions by promoting self-association and/or structural organization of its diverse binding partners. This work addresses the mechanistic and structural features of LC8-induced Swallow self-association distant from LC8 binding. Mutational design based on a hypothetical helical wheel, inter-monomer NOEs assigned to residues expected at interface positions and circular dichroism spectral characteristics indicate that the LC8-promoted dimer of Swallow is a coiled-coil. Secondary chemical shifts and ^{15}N backbone relaxation identify the boundaries and distinguishing structural features of the coiled-coil. Thermodynamic analysis of Swallow polypeptides designed to decouple self-association from LC8 binding reveals that the higher binding affinity of the engineered bivalent Swallow is of purely entropic origin and that the linker separating the coiled-coil from the LC8 binding site remains disordered. We speculate that the LC8-promoted coiled-coil is critical for *bicoid* mRNA localization because it could induce structural organization of Swallow, which except for the central LC8-promoted coiled-coil is primarily disordered.

Swallow is a 62 kDa multi-domain protein with a predicted α-helical coiled-coil centered between primarily disordered N- and C-terminal domains (Figure 1). Synthesized by maternal nurse cells in the egg chamber, Swallow is exported to the interconnected oocyte compartment during *Drosophila* oogenesis (1–3), where it is required for proper localization of several mRNAs such as *bicoid* mRNA (*bcd* mRNA), *huli-tai shao*-adducin-like mRNA (*htsN4* mRNA), and Oskar (4, 5). *Bcd* mRNA localization in the anterior cortex of the *Drosophila* oocytes establishes a morphogenetic gradient of bicoid protein, which determines the anterior-posterior embryonic pattern (6, 7). In Swallow mutants with deletions in the predicted coiled-coil domain or truncations in the C-terminal domain, *bcd* mRNA fails to localize but spreads uniformly throughout the oocyte cytoplasm resulting in embryonic anterior defects (1). Additionally, Swallow mutants affect mislocalization of *htsN4* mRNA causing cytoskeleton anomalies and consequent nuclear cleavage and migration defects (4).

[*]Corresponding author: Elisar Barbar, Department of Biochemistry and Biophysics, Oregon State University, Corvallis, OR 97331. Tel: 541-737-4143, Fax: 541-737-0481, barbare@science.oregonstate.edu.
[3]Current address: Pfizer Global Research and Development, Eastern Point Road, Groton Connecticut

Swallow sequence analysis revealed a recognition sequence for dynein light chain LC8 at the C-terminal end of the predicted coiled-coil (1). LC8 (DYNLL1 in mammals) is a highly conserved 10.3 kDa homodimeric protein that assembles in the molecular motor dynein by binding intermediate chain IC (8–10). LC8 was first described in dynein and was widely viewed as a dynein cargo adaptor (11). Binding of Swallow to LC8 fostered the hypothesis that *bcd* mRNA cargo is transported by dynein through its interaction with Swallow (1, 3). However, crystal structures of LC8 bound to Swallow and IC peptides later showed that both partners bind the same symmetrical grooves at the LC8 dimer interface (8, 12, 13). Moreover, LC8 in both cases binds two chains of the *same* protein and promotes their self-association distant from the LC8-Swallow interface (9, 14) arguing against the one groove one peptide model (15); therefore, LC8 cannot simultaneously bind to dynein and to Swallow, implying both dynein and dynein-independent LC8 functions (8, 16). Consistent with dynein-independent LC8-Swallow association, recent reports indicate that Swallow and *bcd* mRNA are transported independently and *bcd* mRNA along with the protein Staufen are carried by dynein to the anterior pole, where Swallow is already localized (17). Instead of directly binding to *bcd* mRNA and dynein, Swallow appears to be involved in the stabilization of microtubules associated with transport of *bcd* mRNA (4, 17, 18).

What exactly is the role of LC8 in the LC8-Swallow interaction? Insight into this question is given from an analysis of LC8 and over 20 LC8-partner proteins involved in essential and diverse cellular processes (16), including chromosome segregation, mitotic spindle assembly (19) and apoptosis (20), where LC8 deletion or overexpression causes cell apoptosis or breast cancer cell malignancy (20, 21). These diverse interactions led to the hypothesis that LC8 functions as a regulatory hub protein in a number of essential systems by facilitating the assembly and stabilization of its primarily disordered partners (16). Such a role was clearly demonstrated for LC8 interaction with dynein IC and with the nuclear pore complex subunit Nup159: in both instances, LC8 binding promotes self-association and higher order assembly of its partners (22–24). In the case of Swallow, biophysical characterization of its predicted coiled-coil domain shows that this domain is primarily monomeric at room temperature and that LC8 binding is required for its self-association and stability (the melting temperatures with and without LC8 are 15 °C and 45 °C, respectively) (14).

Here we expand our studies of the LC8-Swallow interface (8, 12) and the observation that LC8 promotes Swallow self-association (14) to identification of the structural features of the self-association domain promoted by LC8 and the mechanism for its formation. We demonstrate by mutational design and inter-monomer NOEs that the self-association domain is coiled-coil as predicted and identify by secondary chemical shifts and backbone dynamics the boundaries and distinguishing structural features of this domain. Thermodynamics analysis of Swallow constructs designed to decouple self-association from LC8 binding reveals that LC8 binding enhances self-association by the entropic bivalency effect, and gives a measure of the extent of self-association. Since the residues predicted to form a coiled-coil domain are essential for proper functioning of Swallow (1), our working model is that LC8 binding promotes formation of the coiled-coil, which in turn is necessary for regulation of long-range events associated with structural organization of the disordered N- and C-terminal domains.

Materials and Methods

Constructs Design and Protein Preparation

The regions corresponding to Swallow residues 205 – 275, and 206 – 297 were amplified by PCR and subcloned into the Champion™ pET –SUMO (Invitrogen) or pET 15 (Novagen) vectors respectively. Multi-site-directed mutagenesis was performed to generate Swa_{DIMER}(206–297), $Swa_{MONOMER}$(206–297), and Swa_{DIMER}(205–275) with two (R224E/

K244I), three (F206K/I220K/C265K), and four (R224E/K244I/C253D/C265A) mutations respectively. Two co-expressed constructs were also generated by subcloning LC8 or its phosphomimetic mutant (S88E) (25) with Swa_{WT} (aa 206–297) into a pETDuet-1 co-expression vector (Novagen). The sequences of all constructs were verified prior to transformation into *E. coli* BL21 (DE3) for protein expression.

Cells were grown at 37 °C in LB for Swa_{WT}, Swa_{DIMER}(206–297), $Swa_{MONOMER}$(206–297), pETDuet-1 Swa_{WT}/LC8 and Swa_{WT}/LC8-S88E, or MJ9 media containing $^{15}NH_4Cl$ and ^{12}C or ^{13}C glucose for Swa_{DIMER}(205–275) to OD_{600} of 0.6 – 0.8. Protein expression was induced by 0.2 mM isopropyl β-D-galactopyranoside, and cells were grown for an additional 4 h at 37 °C for $Swa_{MONOMER}$(206–297) or 16 h at 18 °C for Swa_{DIMER}(206–297), Swa_{DIMER}(205–275), Swa_{WT}/LC8 and Swa_{WT}/LC8-S88E. Cells were harvested, resuspended in lysis buffer (50 mM sodium phosphate pH 8.0, 500 mM NaCl, 10 mM imidazole, 5 mM β-mercaptoethanol and a protease inhibitor cocktail), disrupted by sonication, centrifuged, and the protein purified using Ni-NTA affinity resin (Qiagen). $Swa_{MONOMER}$(206–297) expressed in inclusion bodies was purified under denaturing conditions. The SUMO tag of the Swa_{DIMER}(205–275) was removed following Invitrogen's protocols. After final purification on a Superdex™ 75 (16/60) column (GE Healthcare), the proteins were dialyzed in appropriate buffers and their purity and molecular weights were confirmed by MALDI-TOF mass spectrometry. Protein concentrations were determined from absorbance at 280 nm as in (14).

Size Exclusion Chromatography and Multi Angle Laser Light Scattering

The association state(s) of Swa_{DIMER}(206–297) and $Swa_{MONOMER}$(206–297) mutants were determined from analytical size-exclusion chromatography on a Superdex 75 HR analytical column (GE healthcare) with an online multi-angle laser light scattering detector (miniDawn, Wyatt Technology). The running buffer was 200 mM sodium sulfate, 50 mM sodium phosphate, 1 mM sodium azide at pH 7.3 and 5 mM β-mercaptoethanol. 100 or 200 μl of protein samples were injected at a flow rate of 0.5 ml/min at room temperature at a loading protein concentration in the 100–500 μM range. Samples were monitored by UV absorption at 220 or 280 nm and by refractive index. For Swa_{DIMER}(205–275), several buffer conditions were tested to identify 20 mM MES, 10 mM NaCl at pH 5.6 as the appropriate buffer that gives a homogeneous dimer with no higher aggregates at concentrations suitable for NMR studies. The MALLS-determined molecular weight of Swa_{DIMER}(205–275) is 20 kDa, consistent with the theoretical value of 18 kDa expected for a dimer. Data were processed using ASTRA v5.1.9.1 (Wyatt Technology).

Circular Dichroism

CD spectra were collected on a Jasco720 spectropolarimeter using a water bath and water-jacketed cells for temperature control. Samples were prepared in 10 mM sodium phosphate buffer with 30 mM NaCl, pH 7.8 in the protein concentration range of 3–30 μM. Thermal unfolding was measured by monitoring the CD signal at 222 nm in the temperature range of 5–83 °C, allowing 3 minutes of equilibration per 3 °C temperature increment. Reversibility was determined by comparing measurements taken at 5 °C before and after thermal unfolding. The fraction of folded $Swa_{MONOMER}$(206–297) was determined from comparison to the CD signal of Swa_{DIMER}(206–297) at similar concentrations.

Isothermal Titration Calorimetry

Proteins were dialyzed in PBS buffer containing an additional 5 % (v/v) glycerol, 5 mM β-mercaptoethanol and 1 mM benzamadine at pH 7.4. Thermodynamics of binding were determined at 20, 25, 30 and 35 °C using a VP-ITC isothermal titration calorimeter from MicroCal (Northampton, MA), and processed using Origin 7.0 (OriginLab Corp.,

Northampton, MA). Data were fit to a single-site binding model, A + B →AB, where A and B refer to a single chain of Swallow and LC8, respectively. Heat of dilution, estimated to be less than the enthalpy of the final injection, was subtracted from the data prior to fitting.

All ITC experiments were conducted with Swallow proteins in the sample cell and LC8 in the syringe using cell/syringe concentrations of 0.003/0.1, 0.03/0.5 and 0.02/0.5 mM for Swa_{WT}/LC8, $Swa_{MONOMER}$(206–297)/LC8 and Swa_{DIMER}(206–297)/LC8, respectively. The "c-value" ($c = [protein]_{sample\ cell} \times K_d^{-1}$) was between 3–30, 30–85, and 17–420 for Swa_{WT}, $Swa_{MONOMER}$(206–297) and Swa_{DIMER}(206–297), respectively. The c values for the interactions with Swa_{WT} are the lowest due to its limited solubility. Changes in heat capacity at constant pressure (ΔCp) were determined from the slope of the change in enthalpy (ΔH◦) as a function of temperature. All ΔCp values were obtained with linear correlation coefficients of 0.93 or greater.

NMR Experiments and Analysis

Doubly labeled $^{15}N/^{13}C$ samples of Swa_{DIMER}(205–275) were prepared at a protein concentration of 0.5 mM in MES buffer (20 mM MES, 10 mM NaCl, 1 mM sodium azide, pH 5.6), protease inhibitors and 4,4-dimethyl-4-silapentane-1-sulfonic acid (DSS) for referencing of ^{1}H chemical shifts. ^{1}H-^{15}N HSQC spectra were collected at 10, 20, 30, and 40 °C with the spectrum at 40 °C showing the best resolution and highest number of peaks. Therefore, all subsequent experiments were collected at 40 °C.

A series of BEST–TROSY NMR experiments (26) including HNCACB, HN(CO)CACB and TROSY- H(CCCO)NH-TOCSY, (H)CC(CO)NH-TOCSY, HAHB(CBCACO)NH were collected for backbone assignment on Bruker spectrometers in the field range of 600–950 MHz. NMR spectra were processed with TopSpin (Bruker) and analyzed with Sparky (27) or NMRView (28).

Secondary structure propensities for Swa_{DIMER}(205–275) were determined from the program SSP using the Cα, and Cβ chemical shifts (29). Negative scores correspond to β-strands while positive scores correspond to α helices (29). Coiled-coil prediction of Swa_{DIMER}(205–275) was performed using Coils (30).

NMR dynamics data were derived from the measurement of ^{15}N relaxation experiments including R_1, R_2 and steady-state heteronuclear NOE on a Varian 800 MHz instrument. R_1 and R_2 relaxation experiments were collected at 40 °C at time points: 0, 100, 200, 400, 600, 800, 1100, 1500, 1900 ms for R_1, and at 30, 50, 70, 90, 100, 130, 170, 210, and 250 ms for R_2. R_1 and R_2 values were determined by fitting peak heights versus time profiles to the formula: $I = I_0*\exp(-t*R)$ using the rate analyses interface in NMRView (28), where I_0 is the initial peak intensity and I is the intensity measured at time t. Curve fitting and standard deviations were calculated by NMRView (28). NOE values were obtained from the ratios of peak intensities in the presence and absence of amide proton saturation. Standard deviations were determined from the intensities of the baseline noise using the formula $\sigma/(NOE) = [(\sigma I_{sat}/I_{sat})^2 + (\sigma I_{unsat}/I_{unsat})^2]^{1/2}$, where I_{sat} and σI_{sat} correspond to the intensity of the peak and its baseline noise.

A 3D ω1-$^{13}C/^{15}N$-filtered, ^{13}C-separated NOESY-HSQC spectrum (31) was collected at 900 MHz on a Swa_{DIMER}(205–275) sample prepared by mixing equimolar amounts of $^{13}C/^{15}N$-labeled and unlabeled protein in 4 M urea, 50 mM phosphate, 150 mM NaCl, and pH 8.0. The dimeric protein was then reconstituted by dialysis in 20 mM MES, 10 mM NaCl pH 8.0 and concentrated to 0.8 mM.

Results

Design of Swallow Constructs that Promote or Disrupt Coiled-Coil Stability

The construct Swa(206–297) (referred to as Swa_{WT}) includes the predicted coiled-coil (residues 206–275) and the LC8 recognition sequence (residues 287–296) (8, 14). The construct Swa_{DIMER}(206–297) includes two mutations that promote coiled-coil stability: R224 (position *e* on a hypothetical helical wheel, Figure 1b) was replaced with Glu (turquoise) to minimize charge-charge repulsion upon interaction with K219 at position *g* of the opposite chain, and K244 (position *d*) was replaced with Ile (turquoise) to remove a charged residue from the putative hydrophobic interface upon coiled-coil formation. The construct $Swa_{MONOMER}$(206–297) includes three mutations that disrupt coiled-coil formation: F206 and I220 (both at positions *a*) and C265 (position *d*) were all replaced with Lys (yellow) which inhibits formation of coiled-coil to avoid charge-charge repulsion at the interface. To facilitate structural studies at concentrations suitable for NMR, a shorter construct which contains only the predicted coiled-coil domain Swa_{DIMER}(205–275) was made. Swa_{DIMER}(205–275) is a model of the LC8-bound Swallow as it includes the R224E and K244I dimer stabilizing mutations. Additionally it includes the C253D and C265A (green) mutations that prevent aggregation caused by disulfide bond formation at NMR concentrations.

Association State(s), Structure and Stability

Association states of Swallow mutants were determined from size exclusion chromatography and multi-angle laser light scattering (MALLS). Figure 2a shows a single peak for each of $Swa_{MONOMER}$(206–297) and Swa_{DIMER}(206–297) with MALLS-determined molecular weights in good agreement with theoretical molecular weights (14.7 kDa experimental *v* 13.3 kDa theoretical for a monomer) and (27.7 kDa experimental *v* 26.6 kDa theoretical for a dimer).

Circular dichroism (CD) differentiates between single and supercoiled helices based on the ratio of ellipticity at 222 and 208 nm. CD spectra of $Swa_{MONOMER}$(206–297), Swa_{DIMER}(206–297) and Swa_{WT} are shown in Figure 2b. While both Swa_{DIMER}(206–297) and Swa_{WT} show double minima at 208 and 222 nm characteristic of an α-helical conformation, Swa_{DIMER}(206–297) has a higher $[\theta_{222}]/[\theta_{208}]$ ratio (close to 1), characteristic of supercoiling and similar to the spectra of LC8 bound to Swa_{WT} (14). $Swa_{MONOMER}$(206–297) in contrast shows limited signal at 222 nm and a strong negative peak at 201 nm indicative of a primarily disordered protein. No increase in CD-detected structure was observed in the 10–30 μM concentration range (spectrum in Figure 2b was collected at 30 μM). At 5 °C, a small increase in helical structure is inferred from an increase in negative ellipticity at 222 nm (Figure 2c) and a small shift in the minima from 201 to 203 nm (data not shown).

The relative stabilities of Swa_{DIMER}(206–297) and $Swa_{MONOMER}$(206–297) were determined from their melting curves at 222 nm (Figure 2c). $Swa_{MONOMER}$(206–297) is fully unfolded above 25 °C, while Swa_{DIMER}(206–297) is considerably more stable and does not detectably unfold below 60 °C. Superimposable melting curves for protein concentrations of 3 μM and 30 μM indicate a stable dimer at concentrations above 3 μM (data not shown).

Interactions of LC8 with Swallow

Co-expression of LC8 with Swa_{WT} significantly increases the recombinant expression of soluble Swa_{WT}. The co-expressed LC8/Swa_{WT} complex elutes as a single peak on a gel filtration column (data not shown) consistent with tight binding between LC8 and Swa_{WT}

and has a MALLS determined molecular weight of 50 kDa, in good agreement with the 47.8 kDa theoretical mass for a 1:1 complex of dimeric LC8 and dimeric Swallow.

The thermodynamics of LC8 binding to Swallow constructs were measured by isothermal titration calorimetry (ITC) (Figure 3). Association parameters (ΔG°, ΔH°, $-T\Delta S^\circ$) are given in Table 1 and Figure 4. LC8 binds Swa_{WT} with moderate affinity (K_d of 200 nM at 25 °C), significantly tighter than LC8 binding to $Swa_{MONOMER}$(206–297) (K_d of 500 nM), but considerably weaker than binding to Swa_{DIMER}(206–297) (K_d of 70 nM). All interactions are enthalpically driven (Figure 3 and Table 1). Interestingly, the enthalpy change of binding is the same for both $Swa_{MONOMER}$ and Swa_{DIMER} (−12.2 kcal/mol), and is significantly less than that of Swa_{WT} (−15.2 kcal/mol), which has the highest favorable enthalpy change and highest unfavorable entropy change. Swa_{DIMER}(206–297) binds LC8 with 7-fold binding enhancement relative to the comparable interaction with $Swa_{MONOMER}$(206–297) ($\Delta\Delta G^\circ$ of −1.1 kcal/mol) (Figure 4).

Enthalpy of binding measurements in the 20–35 °C range give heat capacity ΔCp values of −0.52 for Swa_{WT} and −0.15 kcal/mol/K for both Swa_{DIMER}(206–297) and $Swa_{MONOMER}$(206–297) (Figure 4 and Table 1). Indistinguishably small ΔCp values for Swa_{DIMER}(206–297) and $Swa_{MONOMER}$(206–297) are likely due to sequestration from solvent of atoms at the LC8/Swallow interface. The larger ΔCp of −0.52 for Swa_{WT} reflects additional transfer from solvent or adoption of ordered structure distant from the LC8/Swallow interface.

NMR Analysis of Swa_{DIMER}(205–275)

The ^{1}H-^{15}N HSQC spectrum of Swa_{DIMER}(205–275) with amide backbone resonance assignments of 69 out of the expected 71 residues is shown in Figure 5. Secondary structure propensities (SSP) calculated from Cα and Cβ chemical shifts (Figure 6a) show that residues 216–234 and residues 249–265 have the highest positive SSP scores indicating the strongest helical propensity. Residues in the middle (235–248) have a relatively lower SSP scores which interestingly correspond to residues with weaker coiled-coil prediction (the white segment of the bar at the top of Figure 6). Much lower SSP scores mark both termini indicating disorder at the chain ends.

Backbone dynamics of Swa_{DIMER}(205–275) were determined from ^{15}N R_1 (longitudinal), R_2 (transverse) relaxation and steady-state heteronuclear NOE spectra. R_1 values, which provide information on the overall molecular motions, are higher at the N and C-termini and for residues 220, 238, 243, indicating more flexibility and heterogeneity in these regions relative to the rest of the protein (Figure 6b). R_2 values which are sensitive to internal motions are lower at both the N and C termini indicating large-amplitude backbone motions on the sub-nanosecond timescale, consistent with disordered structure (Figure 6c). Additionally, relatively low R_2 values for some residues and a non-uniform R_2/R_1 ratio within the sequence indicate significant heterogeneity in the middle regions. Negative NOE values at the C terminal indicate full disorder (Figure 6e).

In dimeric coiled-coils, the major contributors to inter-monomer NOEs are expected to involve residues at the *a* and *d* positions of the heptad repeats, as these positions are occupied by hydrophobic amino acids packed in a “knob to holes” manner to form a super coiled α-helix. About 25 inter-monomer NOEs were observed in a 3D $\omega 1$-$^{13}C/^{15}N$-filtered, ^{13}C separated NOESY-HSQC spectrum from which 13 were unambiguously assigned. ^{13}C-^{1}H inter-monomer NOE peak strips are shown for those that are assigned and mapped as a discontinuous stretch to the *a* and *d* positions along the length of the predicted coiled-coil (Figure 7).

Discussion

Binding of LC8 Assists Swa_{WT} Folding

The Swa_{WT} construct, expressed primarily in inclusion bodies, has limited solubility (<10 μM) and is primarily monomeric and disordered at physiological temperature (14). In contrast, Swa_{WT} co-expressed with LC8 is produced in high yield and is soluble even at >500 μM concentration, an indication that LC8 binding aids folding and solubility of Swa_{WT} during expression in the cell, and *in vitro* after purification. This increase in solubility is not observed when Swa_{WT} is co-expressed with $LC8_{S88E}$, a phosphomimetic mutant of LC8 with weak binding to Swa_{WT}, suggesting that tight binding of LC8 facilitates *in vivo* Swallow folding and protection from aggregation.

The Swallow Self-association Domain Is a Coiled-coil

Engineered stabilizing mutations based on a hypothetical coiled-coil helical wheel result in a stable dimer, Swa_{DIMER}(206–297), with a melting profile (Figure 2c) that is suggestive of dissociation coupled to unfolding, characteristic of a stable coiled-coil/leucine zipper dimer (32). This is in contrast to the two-step melting profile observed for Swa_{WT} which is an equilibrium mixture of temperature dependent monomer and dimer (14). Engineered destabilizing mutations designed based on a hypothetical coiled-coil helical wheel result in a fully monomeric and primarily unfolded protein. The stability behavior of variants produced with the design assumption of a coiled-coil strongly supports the conclusion that in the naturally occurring sequence this domain acquires a coiled-coil configuration that is in register with a wheel based on the predicted coiled-coil.

Swa_{DIMER}(205–275) has a thermal stability and dissociation profile similar to the LC8-bound Swa_{WT} and due to the relative ease of its NMR characterization, Swa_{DIMER}(205–275) is used as a model for Swa_{WT} when bound to LC8. The NMR secondary chemical shifts indicate highest helical propensities for residues 216–234 and 249–265, relatively lower for residues 207–215 and 235–248 and full disorder for C-terminal segment 270–275. Inter-monomer NOEs are consistent with the hypothetical wheel for a dimeric coiled-coil. Dynamic measurements indicate disorder at the termini and some heterogeneity in the middle regions. Other evidence in support of a coiled-coil is the elongated structure inferred from hydrodynamics measurements, and the supercoiling from circular dichroism spectra (Figure 2b). In the absence of a 3D structure, a truly challenging task for coiled-coil domains of this size, these data provide strong indication of a coiled-coil self-association mode for Swallow, with some deviation from standard coiled-coil structure for middle residues.

LC8 Binding Is Coupled to Swallow Self-Association

Thermodynamic coupling of LC8 binding and Swallow self-association is manifested by the significantly larger ΔCp associated with LC8 binding to Swa_{WT} (−0.52 kcal/mol/K) relative to Swa_{DIMER}(206–297) and $Swa_{MONOMER}$(206–297) (ΔCp of −0.15 kcal/mol/K for both). Heat capacity is a measure of the extent of the burial and dehydration of molecular surfaces from surrounding solvent molecules upon intermolecular association (33, 34). The 0.37 kcal/mol/K difference in ΔCp suggests that for Swa_{WT}–LC8 binding there is additional folding, rigidity, and/or sequestration of atoms from solvent compared to LC8 binding to fully dimeric and fully monomeric Swallow constructs. This is consistent with the expectations that for Swa_{DIMER}(206–297) a coiled-coil is already formed and for $Swa_{MONOMER}$(206–297) a coiled-coil never forms. The large unfavorable ΔS and large favorable ΔH observed for LC8 binding to Swa_{WT}, compared to LC8 binding to Swa_{DIMER}(206–297) and $Swa_{MONOMER}$(206–297), are consistent with the interpretation that only in Swa_{WT} there are structural changes in the self-association domain upon LC8 binding. However, a −0.37 kcal/mol/K for self-association of the coiled-coil is somewhat lower than expected for a coiled-

coil domain of this size. Heat capacity measurements of heterodimerization of leucine zippers for example, show significantly higher ΔCp (−0.7 for a 30 amino acid peptide to −1.1 kcal/mol/K for a 54 amino acid peptide) (32, 35). ΔCp of unfolding of a homodimeric coiled-coil gives a similar value (about 1 kcal/mol/K for a 30 amino acid peptide) (32). By this measure, a −0.37 kcal/mol/K value would correspond to formation of tightly packed 16–18 amino acids out of the predicted 60 amino acids. One explanation for the lower than expected ΔCp value for formation of a coiled-coil of this size is that a percentage of the Swa_{WT} is already dimeric and the −0.37 value is a measure of only about 70% of the total population. Another is that the monomer is not fully unfolded as in the model coiled-coil proteins studied and therefore there is already some sequestration from solvent in the monomer before self-association. A third is that the coiled-coil formed is not as tightly packed as the Fos/Jun leucine zipper for example. Destabilizing interactions as those observed in Swa_{WT} (between K219 and R224, and due to positioning of K244 at the hydrophobic interface) could contribute to a lower ΔCp (36). The present NMR dynamics data confirm a helical coiled-coil structure along the length of the predicted coiled-coil but also show significant heterogeneity within the coiled-coil. Taken together, the most likely interpretation is that the presence of a pre-existing dimer and the heterogeneity within the entire coiled-coil together contribute to the lower ΔCp value.

Another important observation of the thermodynamics is the similarity in ΔCp values between the engineered monomer and dimer. This is an indication that there is no sequestration from solvent except at the LC8 site implying that the linker separating the LC8 site from the coiled-coil remains disordered.

Poly-bivalency in LC8-Swallow Interactions

Binding enhancement arising from bivalency is implied from the difference in LC8 affinity for Swa_{DIMER}(206–297) versus $Swa_{MONOMER}$(206–297). Both proteins are expected to adopt the same β-strand structure at the LC8/Swa interface, and to differ in their structure distant from the LC8 binding sequence. Swa_{DIMER}(206–297), a tightly associated coiled-coil, is a bivalent binding partner with two aligned recognition sequences for LC8. $Swa_{MONOMER}$(206–297) is a disordered monovalent chain with one LC8 recognition motif (Figure 8). A 17-residue linker separates the end of the coiled-coil (residue 270, this work) from the beginning of the LC8 site (residue 287) (8). The binding enhancement of 7-fold is primarily of entropic origin (ΔΔG◦ of −1.1 kcal/mol, TΔΔS◦ of −1.2 kcal/mol, and ΔΔH and ΔΔCp of 0) (Figure 4d), as expected from a bivalency effect (37).

Binding enhancement arising from bivalency appears to be common in assembly of protein complexes with high degree of intrinsic disorder. In dynein assembly, binding of the first light chain to a disordered domain of the intermediate chain IC creates a bivalent IC that binds the second light chain with 50-fold enhancement (38). IC recognition sites for the dimeric light chains LC8 and Tctex1 are separated by a 3-residue linker. Also in IC, stabilizing a weak self-association domain C-terminal to the LC8 recognition site results in 6-fold enhancement of LC8 binding (22). In the nuclear pore protein Nup159, LC8 binds a disordered domain located between a Phe-Gly repeat and a predicted coiled-coil domain to form a structure in which five LC8 homodimers align two extended Nup159 chains (24). The first binding event is weak and the bivalency effect is manifested in binding enhancement of successive events (23). We hypothesize that bivalency effects analogous to those in LC8 binding to IC and Nup159 also occur in the case of Swallow. In these examples bivalency involves not only interactions between intrinsically disordered chains and bivalent protein dimers but also self-association of coiled-coil domains. Binding of disordered proteins is associated with a large entropic penalty: the first binding event pays the entropic cost so the second event due to bivalency either significantly enhances binding affinity of the next bivalent ligand (e.g coiled-coil formation and LC8 binding, this work), or

compensates for unfavorable interactions due to repulsive interactions (e.g. the IC/Tctex1 interface (38)) or increase in protein rigidity (e.g. Nup159/LC8 assembly (23)).

Functional Implications

What are the implications for LC8 promoted coiled-coil formation in Swallow function? Genetic experiments on *Drosophila* ovaries show that the distribution of *bcd* mRNA during oogenesis and early embryogenesis depends on the interaction of LC8 with Swallow. A Swallow mutant lacking the coiled-coil domain and the LC8 recognition motif shows no localization of *bcd* mRNA (1). Interestingly, naturally occurring *swa* alleles with mutations in the protein's C-terminal domain also show defects in *bcd* mRNA localization. These mutations abolish correct Swallow localization but not LC8 binding, suggesting that the primarily disordered C-terminal domain plays a critical role in localization. Coiled-coil-mediated protein interactions are involved in a variety of biological processes including vesicle-mediated transport, cellular membrane organization, cytokinesis, and chromosome segregation (39). Dimerization by formation of a coiled-coil either increases avidity for binding partners as in SCAB1 (40) or allosterically promotes formation of a structured domain conducive for binding, such as inducing formation of a voltage gated channel assembly (41). With Swallow, the LC8-promoted coiled-coil suggests an intriguing potential for further bivalency effects that could allosterically induce structural organization of the disordered N- and C-terminal domains, and thus underlie the essential role of LC8-Swallow interactions in *bicoid* localization.

Acknowledgments

This work is supported by NIH grant GM 084276

We acknowledge the support of the nucleic acid and protein core and the mass spectrometry facilities and services core in the OSU Environmental Health Sciences Center (NIH/NIEHS 00210), Adrien Favier at the Institut de Biologie Structurale and the TGIR-RMN-THC Fr3050 CNRS (Grenoble, France), and access to the Research Infrastructure activity in the 7th Framework Programme of the EC (Project number: 261863, Bio-NMR) (Frankfurt, Germany).

Abbreviations

Swa	Swallow
***bcd* mRNA**	bicoid mRNA
Swa_{WT}	Wild-type Swallow construct corresponding to amino acids 206–297
LC8	dynein light chain
IC	dynein intermediate chain
Nup159	nucleoporin 159
ITC	Isothermal Titration Calorimetry
CD	Circular Dichroism
MALLS	Multi-Angle Laser Light Scattering
HSQC	Heteronuclear Single Quantum Coherence
TOCSY	Total Correlation Spectroscopy
NOE	Nuclear Overhauser effect
ΔCp	Change in heat capacity

References

1. Schnorrer F, Bohmann K, Nusslein-Volhard C. The molecular motor dynein is involved in targeting swallow and bicoid RNA to the anterior pole of Drosophila oocytes. Nat Cell Biol. 2000; 2:185–190. [PubMed: 10783235]
2. Schnorrer F, Luschnig S, Koch I, Nusslein-Volhard C. Gamma-tubulin37C and gamma-tubulin ring complex protein 75 are essential for bicoid RNA localization during drosophila oogenesis. Dev Cell. 2002; 3:685–696. [PubMed: 12431375]
3. Hays T, Karess R. Swallowing dynein: a missing link in RNA localization? Nat Cell Biol. 2000; 2:E60–62. [PubMed: 10783251]
4. Meng J, Stephenson EC. Oocyte and embryonic cytoskeletal defects caused by mutations in the Drosophila swallow gene. Dev Genes Evol. 2002; 212:239–247. [PubMed: 12070614]
5. Pokrywka NJ, Fishbein L, Frederick J. New phenotypes associated with the swallow gene of Drosophila: evidence for a general role in oocyte cytoskeletal organization. Dev Genes Evol. 2000; 210:426–435. [PubMed: 11180848]
6. Berleth T, Burri M, Thoma G, Bopp D, Richstein S, Frigerio G, Noll M, Nusslein-Volhard C. The role of localization of bicoid RNA in organizing the anterior pattern of the Drosophila embryo. EMBO J. 1988; 7:1749–1756. [PubMed: 2901954]
7. Driever W, Nusslein-Volhard C. A gradient of bicoid protein in Drosophila embryos. Cell. 1988; 54:83–93. [PubMed: 3383244]
8. Benison G, Karplus PA, Barbar E. Structure and dynamics of LC8 complexes with KXTQT-motif peptides: swallow and dynein intermediate chain compete for a common site. J Mol Biol. 2007; 371:457–468. [PubMed: 17570393]
9. Benison G, Nyarko A, Barbar E. Heteronuclear NMR identifies a nascent helix in intrinsically disordered dynein intermediate chain: implications for folding and dimerization. J Mol Biol. 2006; 362:1082–1093. [PubMed: 16949604]
10. Makokha M, Hare M, Li M, Hays T, Barbar E. Interactions of cytoplasmic dynein light chains Tctex-1 and LC8 with the intermediate chain IC74. Biochemistry. 2002; 41:4302–4311. [PubMed: 11914076]
11. Harrison A, King SM. The molecular anatomy of dynein. Essays in biochemistry. 2000; 35:75–87. [PubMed: 12471891]
12. Benison G, Karplus PA, Barbar E. The interplay of ligand binding and quaternary structure in the diverse interactions of dynein light chain LC8. J Mol Biol. 2008; 384:954–966. [PubMed: 18948118]
13. Williams JC, Roulhac PL, Roy AG, Vallee RB, Fitzgerald MC, Hendrickson WA. Structural and thermodynamic characterization of a cytoplasmic dynein light chain-intermediate chain complex. Proc Natl Acad Sci U S A. 2007; 104:10028–10033. [PubMed: 17551010]
14. Wang L, Hare M, Hays TS, Barbar E. Dynein light chain LC8 promotes assembly of the coiled-coil domain of swallow protein. Biochemistry. 2004; 43:4611–4620. [PubMed: 15078108]
15. Lo KW, Kan HM, Chan LN, Xu WG, Wang KP, Wu Z, Sheng M, Zhang M. The 8-kDa dynein light chain binds to p53-binding protein 1 and mediates DNA damage-induced p53 nuclear accumulation. J Biol Chem. 2005; 280:8172–8179. [PubMed: 15611139]
16. Barbar E. Dynein light chain LC8 is a dimerization hub essential in diverse protein networks. Biochemistry. 2008; 47:503–508. [PubMed: 18092820]
17. Weil TT, Xanthakis D, Parton R, Dobbie I, Rabouille C, Gavis ER, Davis I. Distinguishing direct from indirect roles for bicoid mRNA localization factors. Development. 2010; 137:169–176. [PubMed: 20023172]
18. Stephenson EC. Localization of swallow-Green Fluorescent Protein in Drosophila oogenesis and implications for the role of swallow in RNA localization. Genesis. 2004; 39:280–287. [PubMed: 15287001]
19. Schmidt JC, Kiyomitsu T, Hori T, Backer CB, Fukagawa T, Cheeseman IM. Aurora B kinase controls the targeting of the Astrin-SKAP complex to bioriented kinetochores. J Cell Biol. 2010; 191:269–280. [PubMed: 20937697]

20. Vadlamudi RK, Bagheri-Yarmand R, Yang Z, Balasenthil S, Nguyen D, Sahin AA, den Hollander P, Kumar R. Dynein light chain 1, a p21-activated kinase 1-interacting substrate, promotes cancerous phenotypes. Cancer Cell. 2004; 5:575–585. [PubMed: 15193260]
21. Rayala SK, den Hollander P, Manavathi B, Talukder AH, Song C, Peng S, Barnekow A, Kremerskothen J, Kumar R. Essential role of KIBRA in co-activator function of dynein light chain 1 in mammalian cells. J Biol Chem. 2006; 281:19092–19099. [PubMed: 16684779]
22. Nyarko A, Barbar E. Light chain-dependent self-association of dynein intermediate chain. J Biol Chem. 2011; 286:1556–1566. [PubMed: 20974845]
23. Nyarko A, Song Y, Novacek J, Zidek L, Barbar E. Multiple recognition motifs in nucleoporin Nup159 provide a stable and rigid Nup159-Dyn2 assembly. J Biol Chem. 2013; 288:2614–2622. [PubMed: 23223634]
24. Stelter P, Kunze R, Flemming D, Hopfner D, Diepholz M, Philippsen P, Bottcher B, Hurt E. Molecular basis for the functional interaction of dynein light chain with the nuclear-pore complex. Nat Cell Biol. 2007; 9:788–796. [PubMed: 17546040]
25. Song Y, Benison G, Nyarko A, Hays TS, Barbar E. Potential role for phosphorylation in differential regulation of the assembly of dynein light chains. J Biol Chem. 2007; 282:17272–17279. [PubMed: 17428790]
26. Lescop E, Kern T, Brutscher B. Guidelines for the use of band-selective radiofrequency pulses in hetero-nuclear NMR: example of longitudinal-relaxation-enhanced BEST-type 1H-15N correlation experiments. J Magn Reson. 2010; 203:190–198. [PubMed: 20031460]
27. Goddard, TD.; Kneller, DG. SPARKY3. University of California; San Francisco:
28. Johnson BA. Using NMRView to visualize and analyze the NMR spectra of macromolecules. Methods Mol Biol. 2004; 278:313–352. [PubMed: 15318002]
29. Marsh JA, Singh VK, Jia Z, Forman-Kay JD. Sensitivity of secondary structure propensities to sequence differences between alpha- and gamma-synuclein: implications for fibrillation. Protein Sci. 2006; 15:2795–2804. [PubMed: 17088319]
30. Lupas A, Van Dyke M, Stock J. Predicting coiled coils from protein sequences. Science. 1991; 252:1162–1164. [PubMed: 2031185]
31. Breeze AL. Isotope-filtered NMR methods for the study of biomolecular structure and interactions. Progress in Nuclear Magnetic Resonance Spectroscopy. 2000; 36:323–372.
32. Jelesarov I, Bosshard HR. Thermodynamic characterization of the coupled folding and association of heterodimeric coiled coils (leucine zippers). J Mol Biol. 1996; 263:344–358. [PubMed: 8913311]
33. Murphy KP, Freire E. Thermodynamics of structural stability and cooperative folding behavior in proteins. Adv Protein Chem. 1992; 43:313–361. [PubMed: 1442323]
34. Spolar RS, Record MT Jr. Coupling of local folding to site-specific binding of proteins to DNA. Science. 1994; 263:777–784. [PubMed: 8303294]
35. Seldeen KL, McDonald CB, Deegan BJ, Farooq A. Thermodynamic analysis of the heterodimerization of leucine zippers of Jun and Fos transcription factors. Biochem Biophys Res Commun. 2008; 375:634–638. [PubMed: 18725194]
36. Steif C, Hinz HJ, Cesareni G. Effects of cavity-creating mutations on conformational stability and structure of the dimeric 4-alpha-helical protein ROP: thermal unfolding studies. Proteins. 1995; 23:83–96. [PubMed: 8539253]
37. Jencks WP. On the attribution and additivity of binding energies. PNAS. 1981; 78:4046–4050. [PubMed: 16593049]
38. Hall J, Karplus PA, Barbar E. Multivalency in the assembly of intrinsically disordered Dynein intermediate chain. J Biol Chem. 2009; 284:33115–33121. [PubMed: 19759397]
39. Wang Y, Zhang X, Zhang H, Lu Y, Huang H, Dong X, Chen J, Dong J, Yang X, Hang H, Jiang T. Coiled-coil networking shapes cell molecular machinery. Mol Biol Cell. 2012; 23:3911–3922. [PubMed: 22875988]
40. Zhang W, Zhao Y, Guo Y, Ye K. Plant actin-binding protein SCAB1 is dimeric actin cross-linker with atypical pleckstrin homology domain. J Biol Chem. 2012; 287:11981–11990. [PubMed: 22356912]

41. Fujiwara Y, Kurokawa T, Takeshita K, Kobayashi M, Okochi Y, Nakagawa A, Okamura Y. The cytoplasmic coiled-coil mediates cooperative gating temperature sensitivity in the voltage-gated H(+) channel Hv1. Nat Commun. 2012; 3:816. [PubMed: 22569364]

42. Jones DT. Protein secondary structure prediction based on position-specific scoring matrices. J Mol Biol. 1999; 292:195–202. [PubMed: 10493868]

43. DeLano, WL. The PyMOL Molecular Graphics System. DeLano Scientific LLC; San Carlos, CA: 2002.

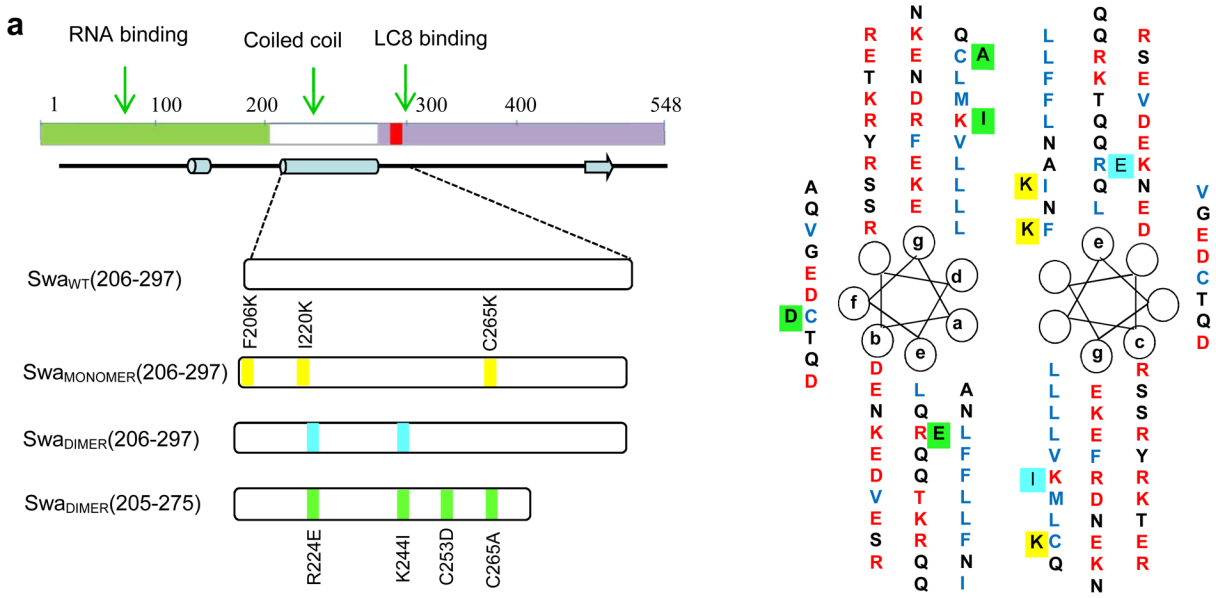

Figure 1.

Schematic representation of full-length *Drosophila* Swallow protein and constructs used in this work. **(a)** Full-length *Drosophila* Swallow includes a putative RNA-binding domain at the N-terminus (green), a predicted α-helical coiled-coil region (residues 205–275) (white), and an LC8 recognition sequence (red) with the canonical motif KATQT (residues 291–295). Predicted secondary structural elements (42) are shown as a cylinder for helix, arrow for strand and solid line for disorder. Site-specific mutations that promote monomer (yellow) or dimer (turquoise, green) formation are indicated on the schematic of the constructs used in this work. **(b)** Hypothetical helical wheel representation of the predicted coiled-coil region. Positions in the heptad repeats are denoted by a–g. Charged, hydrophobic, and neutral residues are shown in red, blue and black respectively. Positions of the monomer- and dimer-promoting mutations are highlighted, yellow and turquoise in one chain and green in the second chain.

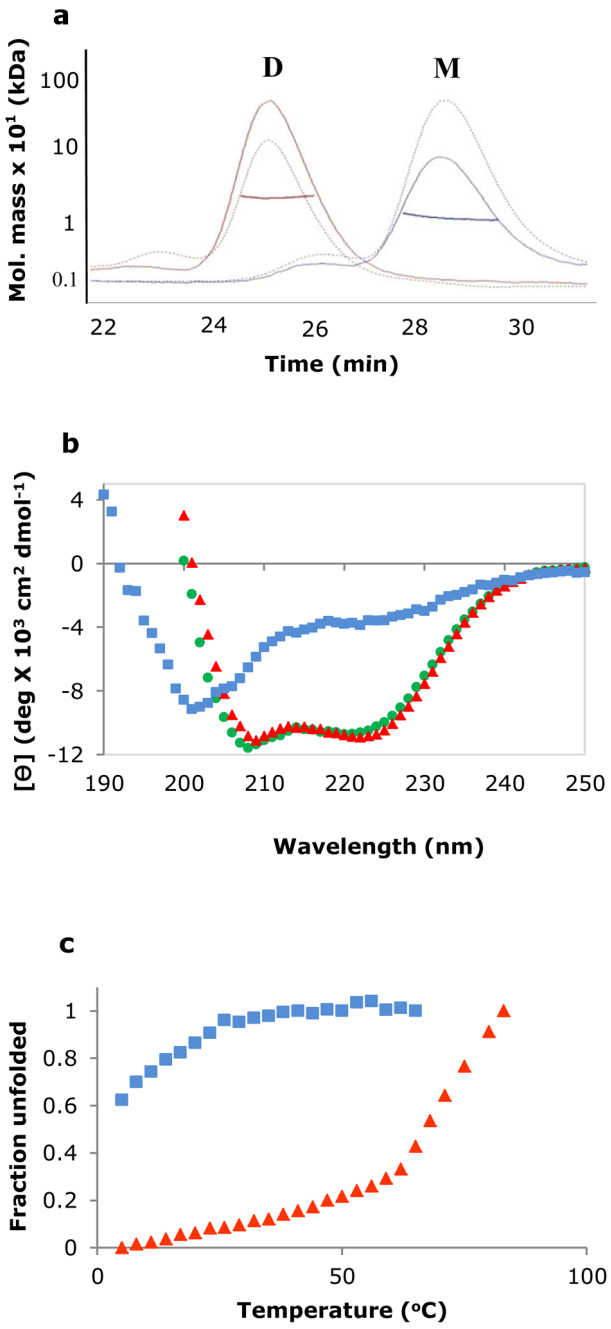

Figure 2.

Association state and stability of Swallow constructs. **(a)** Elution profiles of $Swa_{MONOMER}$(206–297) (M) and Swa_{DIMER}(206–297) (D) shown as overlays of the UV signal at 220 nm and the refractive index. The MALLS analysis is shown as horizontal lines. **(b)** Far UV CD profiles of $Swa_{MONOMER}$(206–297) (blue), Swa_{WT} (green), and Swa_{DIMER}(206–297) (red). **(c)** Thermal unfolding profiles of $Swa_{MONOMER}$(206–297) (blue) and Swa_{DIMER}(206–297) (red) monitored at 222 nm. $Swa_{MONOMER}$(206–297) is predominantly unfolded.

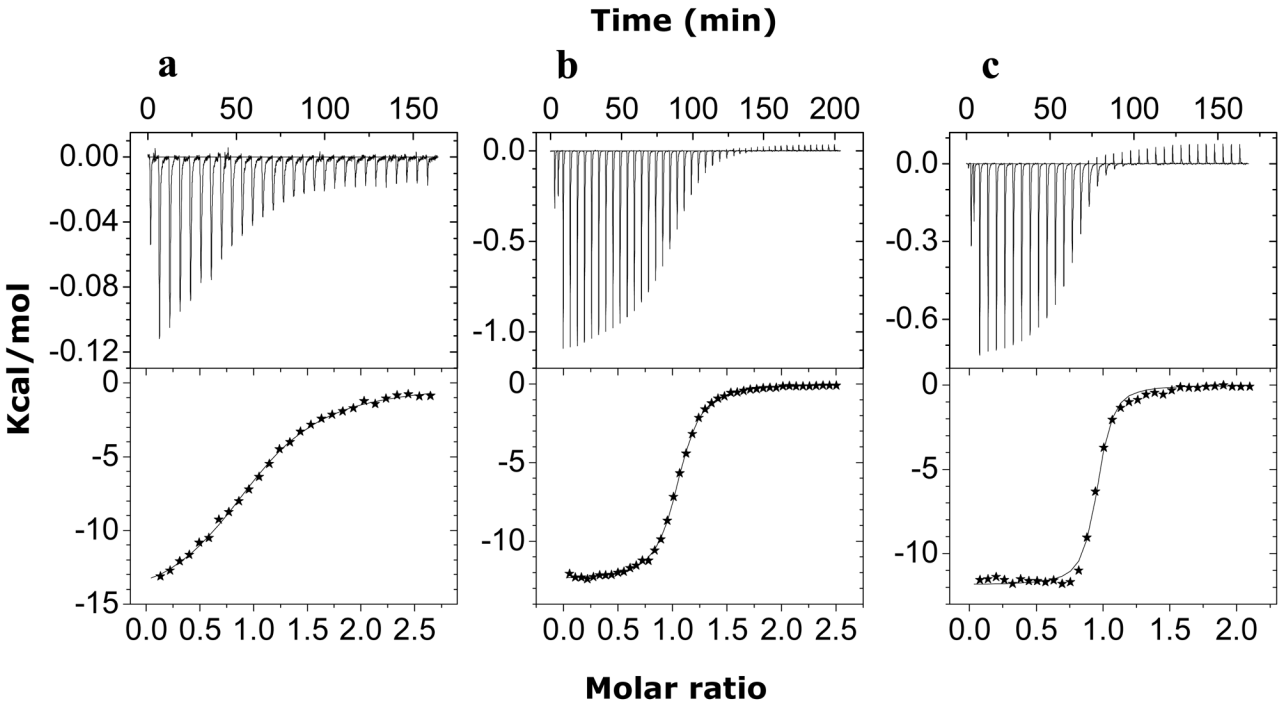

Figure 3.

Representative ITC plots for Swallow-LC8 interactions. Thermograms (top panels) and binding isotherms (bottom panels) are shown for the titration of **(a)** Swa_{WT}, **(b)** $Swa_{MONOMER}$(206–297) and **(c)** Swa_{DIMER}(206–297) with LC8. Data were collected at 25 °C and pH 7.4.

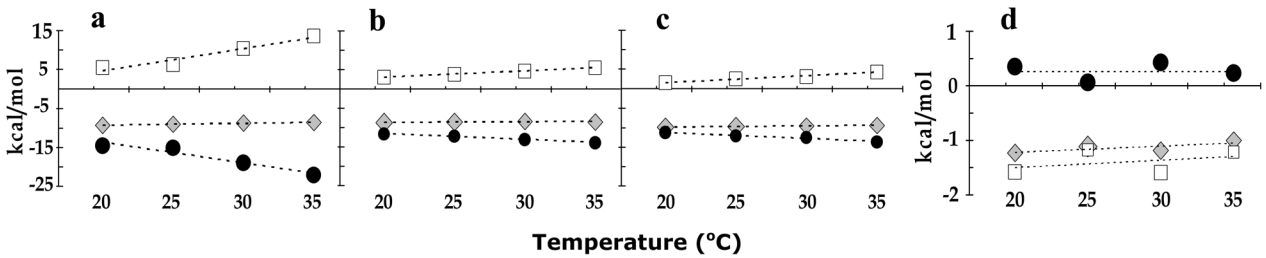

Figure 4.

Plots of thermodynamics association parameters (ΔG◦, grey diamonds; ΔH◦, black circles; and -TΔS◦, white squares) versus temperature for LC8 binding to **(a)** Swa_{WT}, **(b)** $Swa_{MONOMER}$(206–297) and **(c)** Swa_{DIMER}(205–297). The differences in thermodynamic association parameters (ΔΔG◦, grey diamonds; ΔΔH◦, black circles; and -TΔS◦, white squares) versus temperature between LC8 binding to $Swa_{MONOMER}$ **(b)** and Swa_{DIMER} **(c)** are shown in **(d)**.

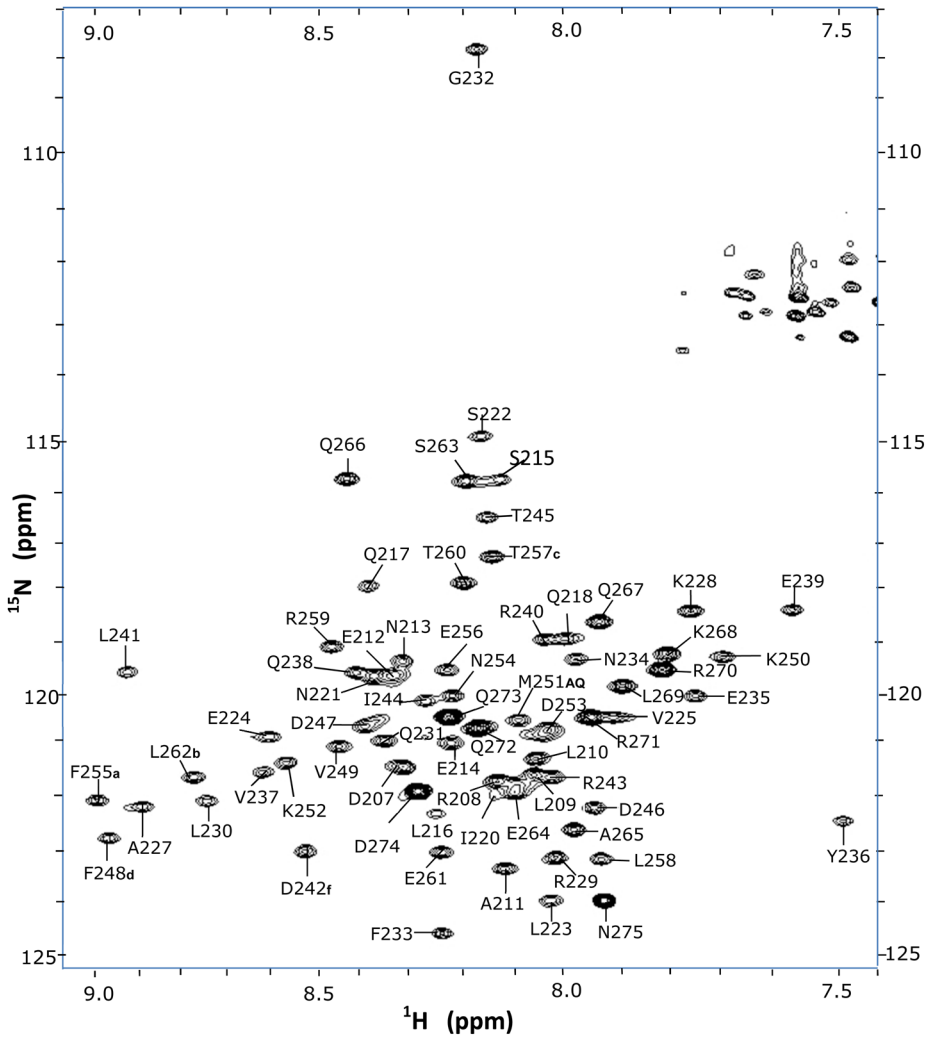

Figure 5.

^{1}H-^{15}N HSQC spectrum of Swa_{DIMER}(205–275) showing assignments. Data were collected at 40 °C on a 950 MHz Bruker Avance III NMR spectrometer.

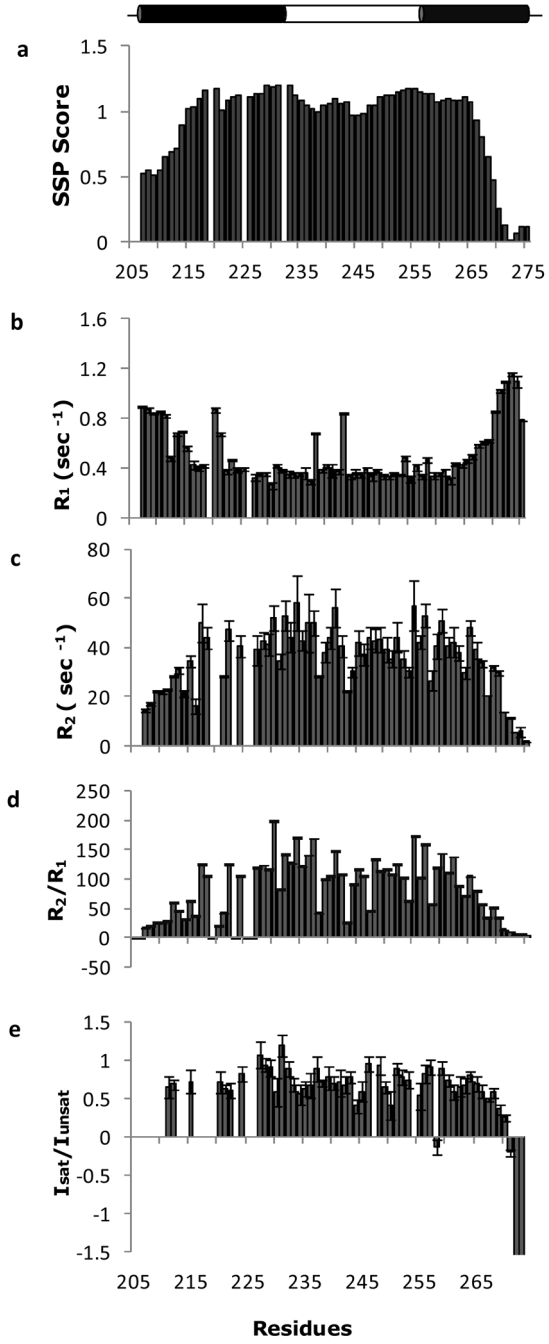

Figure 6.

Secondary structure propensities and dynamics of Swa_{DIMER}(205–275) **(a)** Sequence-based coiled-coil prediction (top bar) show high coiled-coil propensities for residues 206–232 and 256–275 (black), and relatively lower coiled-coil propensities for residues 233–255 (white). Secondary chemical shift determined helical propensities are shown in the bar graph as SSP scores per residue. Plots of R_1, R_2, R_2/R_1 and steady-state heteronuclear NOE obtained at 40 °C are shown in **b, c, d,** and **e,** respectively. In **e,** the steady-state heteronuclear NOE values less than negative 1.5 for the C- terminal residues are truncated.

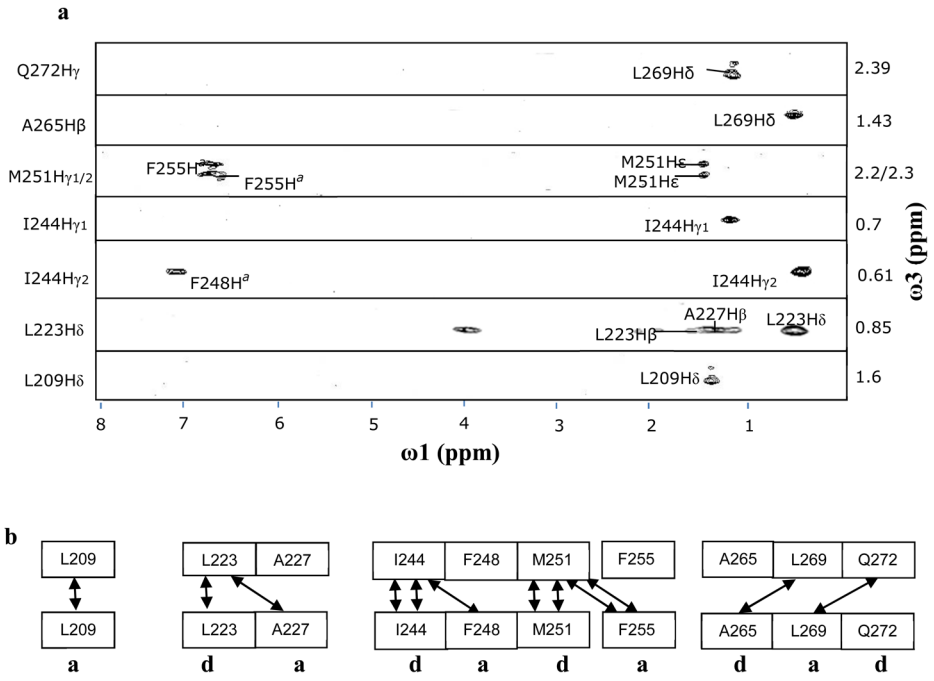

Figure 7.

Assignments of inter-monomer NOEs. **(a)** Select ^{1}H-^{13}C inter-monomer NOE strips from the 3D ω1-^{13}C/^{15}N-filtered, ^{13}C separated NOESY-HSQC spectrum identifying NOEs at the dimer interface of Swa_{DIMER}(205–275). Assignments for aromatic protons are indicated by *a*. **(b)** NOEs across the hypothetical dimeric coiled-coil interface are shown by arrows and correspond to residues at the ‘a’ and ‘d’ positions. Only the NOEs that are unambiguously assigned are shown in this plot.

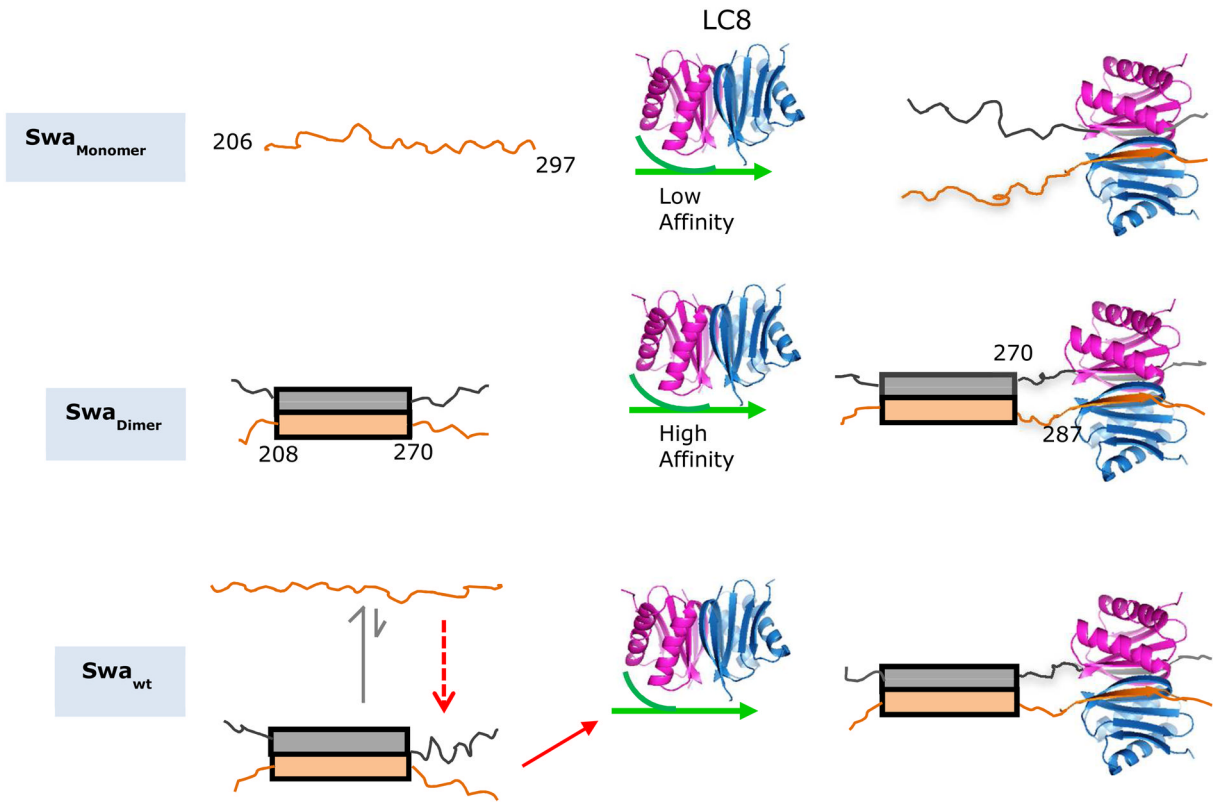

Figure 8.

A model showing LC8 interactions with $Swa_{MONOMER}$(206–297), Swa_{DIMER}(206–297) and Swa_{WT} and demonstrating that burial from solvent distant from the LC8-Swallow interface only occurs with Swa_{WT}. Bars indicate the helical coiled-coil domain and lines indicate disorder. Swa_{WT} is a mixture of high affinity dimer and a low affinity monomer. One model that explains how LC8 binding promotes dimer formation is that LC8 binds the dimeric low population and by mass action shifts the population of the bound to fully dimeric. LC8 and LC8/Swa structures are based on 3BRI and 3E2B pdb codes (12) and were generated using the program PyMOL (43).

Table 1

Thermodynamic parameters for association of Swallow constructs with LC8 at 25 °C[a].

	K_d (nM)	ΔG° (kcal/mol)	ΔH° (kcal/mol)	-TΔS° (kcal/mol)	ΔCp (kcal/mol/K)
Swa_{WT}	200±20	−9.1±0.9	−15.2 ±0.1	6.1 ±1.8	−0.52
Swa_{MONO}	500 ±10	−8.6±0.3	−12.3 ±0.1	3.7 ±0.2	−0.15
Swa_{DIMER}	70 ±10	−9.7±0.6	−12.2 ±0.1	2.5 ± 0.3	−0.15

[a]Average values are reported with error estimated as the standard deviation from three independent measurements.